Observation of multiple dielectric relaxations in BaTiO3-Bi(Li1/3Ti2/3)O3 ceramics

ZHOU, Changrong and FETEIRA, Antonio <http://orcid.org/0000-0001-8151-7009>

Observation of multiple dielectric relaxations in $BaTiO_3$-$Bi(Li_{1/3}Ti_{2/3})O_3$ ceramics

Changrong Zhou[1] and Antonio Feteira[2]

[1]School of Material Science and Engineering, Guilin University of Electronic Technology, Guilin, Guangxi 541004 People's Republic of China

[2]Materials Engineering and Research Institute, Sheffield Hallam University, Howard Street, S1 1WB, Sheffield, United Kingdom

Abstract

Dense $(1-x)BaTiO_3$-$xBi(Li_{1/3}Ti_{2/3})O_3$ ceramics were fabricated by the solid state reaction route. Powder X-ray diffraction analyses revealed an increase in the unit cell volume with increasing x and a change on the average crystal structure from tetragonal (space group *P4mm*) to cubic ($Pm\bar{3}m$) at x> 0.10. Raman spectroscopy analyses corroborated a change of symmetry, but also showed the local structure for x> 0.10 to be inconsistent with the centrosymmetric ($Pm\bar{3}m$) space group. The dielectric measurements revealed for the first time, to our knowledge, a double relaxor behaviour in a $BaTiO_3$-based solid solution. Basically, with increasing x, the sharp ferroelectric anomaly at the Curie temperature (T_c) shifts towards lower temperatures until a relaxor-type response is observed, but simultaneously, another relaxation emerges above T_c. The first arises from poor coupling between polar nanoregions, whereas the later obeys the Arrhenius Law and may be associated either with a defect-dipole reorientation or a Skanavi-type mechanism.

Keywords: Oxides, dielectric properties, Raman spectroscopy

I-Introduction

More than 3 billion multilayer ceramic capacitors (MLCCs) based on $BaTiO_3$ (BT) are annually fabricated, making BT certainly the most successfully commercial and studied lead-free ferroelectric perovskite (ABO_3).[1] Ferroelectricity in BT is believed to arise from a second-order Jahn-Teller distortion caused by the hybridization between the empty Ti d-orbitals and the O p-orbitals.[2] This leads to a correlated off-centering of Ti ions within chains of octahedra. On heating, pure BT undergoes three consecutive structural phase transitions. Basically, its crystal structure changes from rhombohedral to orthorhombic at ~ -80 ^oC, from orthorhombic to tetragonal at ~ 0 ^oC and from tetragonal to cubic at ~ 130 ^oC. These phase transitions are accompanied by large anomalies in ε_r, which are undesirable in most technological applications, particularly in multilayer ceramic capacitors (MLCCs). For instance, ε_r reaches values as high as 10000 around 130 ^oC, the so-called Curie Temperature, T_c. Above T_c, BT is no longer ferroelectric and its ε_r decreases according to the empirical Curie-Weiss law. Chemical doping has been strategically employed to reduce the temperature dependence of ε_r in BT-based ceramics. Nevertheless, most of the dopants added or substituted into the BT lattice tend to lower T_c, limiting the temperature range of its use. Emergence of relaxor behaviour upon doping is another common occurrence, in both single doped systems such as $BaTi_{1-x}Zr_xO_3$[3] (Ti^{4+} and Zr^{4+} are d^0 cations) and double doped systems such as $BaTi_{1-2x}Ga_xNb_xO_3$[4] (Ga^{3+} and Nb^{5+}, d^8 and d^0 cations, respectively). Recently, a so-called weak relaxor behaviour was observed in $(1-x)BaTiO_3$-$xBiMeO_3$ systems, where Me=Sc^{3+} [5](a d^0 cation) or Yb^{3+} [6] (a d^{10} f^{11} cation). This weak-relaxor behaviour is to certain extent independent of the electronic configuration of the B-site dopant. Both systems exhibit a complex but similar dependence of the permittivity maximum with concentration. Indeed, at low doping levels the permittivity maximum shifts towards lower temperatures and becomes rounder, however above a certain doping threshold the permittivity maximum shifts towards higher temperatures. Although this phenomenon can be of potential technological significance, it is still poorly understood. Luisman et al[7] rationalised it as a consequence of a specific lattice disturbance caused by a peculiarity of the doping mechanism, which affects the balance between long-range dipolar Coulombic forces and short-range repulsion forces. Basically, disruption of this balance is responsible for the disappearance of the long-range polar ordering, as indicated by their Raman results. Simultaneously, the presence of Bi^{3+}, with a lone-pair of electrons, leads to localised lattice distortions creating polar nanoregions. Nevertheless, coupling between those polar nanoregions is weak and proper relaxor

behaviour does not develop such as in $Pb(Mg_{1/3}Nb_{2/3})O_3$, a Pb-based B-site complex perovskite. They also postulated that Bi^{3+} should play a key role in the emergence of weak-relaxor behaviour. Interestingly, Schuetz et al[8] also advanced that the lone-pair of electrons in Bi^{3+} determines the peculiar dielectric behaviour of $Bi_{1/2}Na_{1/2}TiO_3$, a Pb-free A-site complex perovskite. Recently, the structure and dielectric properties of $(1-x)BaTiO_3$-$xBi_{1/2}Na_{1/2}TiO_3$ were investigated.[9] It was observed, that both the degree of tetragonality and the Curie Temperature increased with increasing x.

In this work, the structure and the dielectric properties of $(1-x)BaTiO_3$-$xBi(Li_{1/3}Ti_{2/3})O_3$ were investigated. $Bi(Li_{1/3}Ti_{2/3})O_3$ is a putative B-site complex perovskite, as it has never synthesised under normal ambient pressure. Using X-ray diffraction and Raman spectroscopy analyses combined with dielectric measurements the structure-property relationships have been established. Changes on the local crystal symmetry are accompanied by the emergence of two dielectric relaxations. To our knowledge, such double relaxor behaviour was never reported in a $BaTiO_3$-based solid solution.

Experimental

$(1-x)BaTiO_3$-$xBi(Li_{1/3}Ti_{2/3})O_3$ (BBTL) powders were synthesized by standard solid-state reactions. The raw materials used were $BaCO_3$ (>99 %), Bi_2O_3 (>99.9 %), TiO_2 (>99 %), Li_2CO_3 (>99 %),(Sigma Aldrich Co. Milwaukee, WI). Raw materials were weighed according to the $Ba_{1-x}Bi_xTi_{1-x/3}Li_{x/3}O_3$ stoichiometry. Raw materials were mixed in ~250 ml milling bottles, using ~0.5 kg of cylindrical yttria-stabilized zirconia milling media (Dynamic Ceramics, Crewe, UK), together with ~50-60 ml propan-2-ol to a produce slurry. These slurries were then ball milled for ~20 hours and subsequently dried. The resulting powder was passed through a 500 μm sieve. These powders were placed into closed alumina crucibles and calcined first at 600 ^oC for 8 hours and then at 900 ^oC for 8 hours. Powders were milled between calcinations. Reactions at 900 ^oC were repeated until no changes in XRD diffraction data were observed between subsequent cycles. The reacted powders were mixed with 5 % Poly(Ethylene Glycol) Bio Ultra 20000 (Sigma Aldrich Chemical Co, Milwaukee, USA) to act as a binder. These blended powders were then pressed as 13 mm diameter ~1 mm thick pellets using a uniaxial press (Specac, Kent, U.K.). Green pellets were sintered at 1350 ^oC for 2 hours and annealed in air at 800 ^oC for 8 hours. The density of sintered samples was in all cases equal or greater than 93 % of their theoretical density. The densities were measured by the geometric method.

Purity and crystal structure of the ceramics were determined by X-ray powder diffraction using high-resolution diffractometer (CuKα, λ=1.54059 Å, Model D8, Bruker, Coventry, U.K.) operating at 5 kV and 30 mV (Step size 0.01 ^{o} and scan rate of 0.2 ^{o}/min) in transmission geometry.

Raman spectra of sintered BBTL pellets were obtained in backscattering geometry with a Raman spectrometer (Model InVia, Renishaw, New Mills, U.K.) using the 532 nm line of Ar^{+} ion laser as the excitation laser together with a 50 cm^{-1} cut-off filter and a 50× objective to focus on the surface of the ceramics.

Finally, silver paste was applied to both faces of the fired disks to fabricate electrodes suitable for dielectric measurements, which were carried out using an a.c. impedance bridge (Model 1260, Solartron, Farnborough, U.K.) connected to a computer-controlled furnace (Model MTF, Carbolite Ltd, Hope Valley, UK).

Results and Discussion

Structure and Purity

Room temperature X-ray diffraction patterns for $(1-x)BaTiO_3$-$xBi(Li_{1/3}Ti_{2/3})O_3$ ($0 \leq x \leq 0.30$) ceramics are shown in Fig. 1. These data show most ceramics to be consistent with a single phase perovskite, at least within the detection limits of the instrument. All reflections shift continuously towards lower 2θ with increasing x, reflecting an increase in the unit cell volume. Basically, these results support the incorporation of Li^{1+} in the B-site of the BT unit cell, because in 6-fold coordination Li^{1+} ionic radius is 0.76 Å in comparison with 0.605 Å for Ti^{4+}. Moreover, the data show a clear change of crystal symmetry from tetragonal (space group *P4mm*) to cubic (space group $Pm\bar{3}m$) between x=0.10 and 0.20. Basically, for $x \leq 0.10$, the XRD patterns show a clear splitting of the (200)/(002), as illustrated in the inset of Fig. 1, whereas for $x \geq 0.20$ no splitting of reflections is observed. Lattice parameters for x = 0 were calculated as a = 3.9903(6) Å and c = 4.0314(9) Å, which are in good agreement with literature values for $BaTiO_3$ (ICDD no. 5-626). Variation of lattice parameters and unit cell volumes with composition, x, are listed in Table I. Lattice parameters increase continuously, but there is a slight decrease in the unit cell volume when the unit cell changes symmetry. Finally, there is a slightly increase in c/a ratio from 1.0103 for x=0 to 1.0105 for x=0.05,

which is followed by a decrease to 1.0096 for x=0.10. This variation in the degree of tetragonality correlates with a small increase in the Curie Temperature as shown below.

Raman spectroscopy

Room temperature Raman spectra for all BBTL ($0 \leq x \leq 0.30$) ceramics are shown in Fig. 3. The phonon modes in the x = 0 spectrum are assigned according to the work carried out by Pinczuk et al[10] on monodomain $BaTiO_3$ single crystal. In principle, the assignment of phonons as longitudinal (LO) or transverse (TO) optical modes is valid as long the phonon propagates along one of the principal crystallographic directions. In ceramics, the principal crystallographic directions are randomly distributed among the grains. Hence, the Raman modes observed from ceramics result from mixing of A_1 and E modes, resulting into broader modes than those found in single crystals.

In the low- to mid-wavenumber region (< 500 cm^{-1}), the Raman spectrum of pure $BaTiO_3$ shows a broad A_1(TO) mode at ~265 cm^{-1} assigned to BO_6 bending vibrations, an interference dip at ~180 cm^{-1} and a sharp E(TO) "silent" mode at ~305 cm^{-1}.[10] The later mode appears only in presence of reversible long-range polar order, i.e. ferroelectricity. In the high-wavenumber region, the A_1(LO) phonon mode centered at 720 cm^{-1} is often associated with breathing of the oxygen octahedra. This spectrum becomes dramatically affected by the substitution of Ba^{2+} by Bi^{3+} and Ti^{4+} by Li^{1+}, as shown in Fig. 3. Basically, new modes appear at both low- and high-wavenumbers. Moreover, a new interference dip is present at ~140 cm^{-1}, whereas the dip at 180 cm^{-1} is replaced by a new mode. The interference dip at 140 cm^{-1} is due to the presence of two different octahedral environments in the lattice, as suggested by Lu et al[11], and here is caused by Li substitution. It is worth noting that both the antiresonance dip at 180 cm^{-1} and the sharp E(TO) "silent" mode at 305 cm^{-1} are only present in the room temperature spectra of x = 0, x = 0.05 and x = 0.10, but are absent for $x \geq 0.20$, indicating that a high doping levels the long-range ferroelectric order is disrupted. This result suggests the loss of long-range polar ordering with increasing x. In addition, a new phonon mode appears at ~808 cm^{-1}. Although readily visible in the spectrum of x=0.05, its intensity increases with increasing x. This mode is often observed in doped $BaTiO_3$ and it has been ascribed either to B-site dopants or B-site vacancies.[6,12,13] Basically, it is associated with breathing of oxygen octahedra due to the presence of Li^{1+} inside the octahedra. A comprehensive interpretation of the origin of this mode can be found in a recent work by Pokorny et al[14]. The broad A_1(TO) mode (~265 cm^{-1}) shifts remarkably toward higher frequencies. For example, it appears at ~ 298 cm^{-1} in the spectrum of x=0.05. This mode is believed to be associated with the Ti-O

bonds. The shift of the mode at 265 cm^{-1} could be also due to the fact that a large cation (Li) is substituted on the B-site, as observed by Buscaglia et al[15] in Zr-doped BT. Hence, as observed previously in the $BaTiO_3$-$BiYbO_3$ system[6], the presence of a lone-pair of electrons from Bi^{3+} can harden this mode, in contrast with the $BaTiO_3$-$LaYbO_3$ system, where the A_1(TO) mode softens[13]. Moreover, the B-site Jahn–Teller distortion (Ti-site displacement) for octahedra neighbored by Bi^{3+} cations may also be affected by the presence of a lone-pair of electrons, and ultimately the dielectric behavior. Deluca et al[16], showed that in $BaTiO_3$-$Bi_{0.5}Na_{0.5}TiO_3$, the increase in tetragonality and Curie Temperature with increasing Bi content is due to the effect of the lone-pair of Bi forming a bond with one of the oxygens and thereby distorting the octahedral network. This effect can be compensated if a large cation is present at the B-site as shown by Schileo et al[1,17]. The latter could be the case here, given the large ionic radius of Li.

The appearance of new modes at low frequencies (~80 and ~115 cm^{-1}) support the existence of nanosized clusters caused by the simultaneous A-site and B-site substitutions. Moreover these regions (clusters) are sufficiently sized to produce coherent Raman activity. Finally, the spectral similarity between the x = 0.20 and 0.30 suggests that both adopt the same average and local crystal structure, but not truly cubic as inferred from the X-ray diffraction data in Fig. 1. Indeed, no first-order Raman scattering is allowed for the cubic Pm-3m space group, because all atoms are located in sites having a center of inversion. Basically, these two compositions present regions with local deformations, which break the symmetry rules and may have a polar nature. These spectral variations are in agreement with the dielectric behaviour described below.

Dielectric properties

The temperature dependence of the relative permittivity, ε_r, and of the dielectric loss, tan δ, for BBTL ($0 \leq x \leq 0.30$) ceramics measured at 1 MHz in the 30 - 300 ^oC temperature range is illustrated in Fig. 3. According to the overall dielectric behaviour, the samples can be aggregated into two groups. Hence, $x \leq 0.10$ ceramics exhibit clear dielectric anomalies in ε_r, as illustrated in Fig. 3a. For x=0 and 0.05 ceramics, those dielectric anomalies are relatively sharp and their maxima appear at ~128°C and ~130°C, respectively, whereas in x=0.10, the dielectric anomaly is shifted to ~103°C and appears much broader. In contrast, both x=0.20 and 0.30 are characterised by the absence of a clear dielectric anomaly. Instead, the permittivity follows a very depressed curve, which maximum shifts from 76°C for x=0.20 to

115°C to x=0.30. This shift of the permittivity maxima towards higher temperatures has been observed in several double doped $BaTiO_3$ ceramics. Finally, a sudden drop in tan δ between 95°C and 130°C is observed for x≤0.10, whereas broad tan δ peaks are visible for x=0.20 and 0.30 at much higher temperatures, as shown in Fig. 3b.

The frequency dependence of both ε_r and tan δ for x= 0.20 and 0.30 ceramics is illustrated in Fig. 4 and 5, respectively. These samples exhibit two dielectric relaxations in the 30°C to 450°C temperature range. The low temperature relaxation occurs around room temperature. Similar relaxation has been observed in other Bi-doped $BaTiO_3$ and $KNbO_3$ ceramics. Luisman et al[7] postulated that the complex competition between the covalent and ionic bonds in the $KNbO_3$-$BiYbO_3$ system is in the origin of this relaxation. In the present case, the presence of Bi^{3+} and Li^{1+} in the A- and B-sites of the BT lattice provides a similar scenario. Basically, the incorporation of Li^{1+} into the B-site disrupts the Ti-O covalent bonding, which is responsible for the long-range ordered displacement of Ti^{4+}. This is corroborated by the disappearance of the sharp E(TO) "silent" mode at 305 cm^{-1}, as shown on Fig. 2. Moreover, because of the larger ionic radius of Li^{1+} in comparison with Ti^{4+}, large local strains are induced in the lattice structure and symmetry. Similarly, Bi^{3+} ions with lone-pairs of electrons tend to be off-center leading to further local distortions of the lattice. These local distortions are therefore responsible for the appearance of broad modes in the Raman spectra, as shown in Fig. 2, and probably lead to the appearance of polar nanoclusters. Those manifest their existence as new Raman modes at low frequencies, as illustrated in Fig. 2. Hence, the lattice disturbance caused by this doping mechanism affects the balance between long-range dipolar Coulombic forces and short-range repulsion forces, which determines the long-range ferroelectricity in the perovskite structure. The disruption of this balance is responsible for the disappearance of the long-range polar ordering, as indicated by the Raman results and leads to the emergence of the low temperature weak relaxor behaviour, like in the $BaTiO_3$-$BiYbO_3$ and $KNbO_3$-$BiYbO_3$ systems.[6,7] Now to interpret the origin of the high temperature relaxation, it is convenient to characterise the temperature frequency dependence of the dielectric loss. The peak position in the dielectric loss curves illustrated in Fig. 4b and 5b was modelled using the basic Arrhenius equation, as illustrated in Fig. 6. This equation was originally developed to model the dielectric properties of polar liquids and gases and assumes temperature-independent activation energies. The dielectric data can be fitted by the following equation:

$$\nu = \nu_0 exp\left[\frac{-E_a}{k_B T}\right],$$

where ν is the measuring frequency, E_a is the activation energy, k_B is the Boltzmann constant and the pre-exponential ν_0 is the attempt jump frequency. The activation energy of a relaxation phenomenon is different for every system, because it depends on the relaxation mechanism, type and concentration of relaxing entities. It is also worth mention that in general the activation energies increase for increasing concentrations of relaxing entities.

For example, the activation energy for relaxation in relaxors such as $Pb(Mg_{1/2}Nb_{1/2})O_3$ is in the 0.04-0.07 eV range, while for a dipolar glass such as $Rb_{1-x}(NH_4)_xH_2PO_4$ is in the 0.3 to 0.5 eV range. Higher activation energies were reported for relaxations in $BaTiO_3$, which are associated with oxygen vacancies. For example, Warren et al[18] reported an activation energy of 0.91 eV for the alignment of oxygen vacancy-related defect dipoles in the 24-110°C, whereas Fujii et al[19] reported values in the 0.61-0.68 eV range for the same phenomenon in an identical temperature range. Again, Cha and Han[20] reported similar activation energies for defect dipole reorientation in Mg-doped $BaTiO_3$ ceramics in the 150-300°C temperature range, but values greater than 1 eV for oxygen vacancy motion. Finally, Bidault et al[21] reported a value of 1.56 eV for a relaxation associated with a space charge mechanism. In the present work, the activation energies for the relaxation in the 130-320°C temperature range were calculated as 0.747 eV and 0.711 eV for x=0.20 and 0.30, respectively. In principle, such dielectric relaxation can be ascribed to defect dipole reorientation.

Now, let us considered the associated jumping frequencies calculated from the Arrhenius fit. First, the highest anticipated jumping frequency is directly related to the ionic vibration of the lattice, i.e to the Debye frequency, therefore is should not exceed 10^{13} Hz. In the present case, the attempt jump frequencies estimated from the Arrhenius fit are 2.22×10^{12} Hz for x=0.20 and 2.30×10^{12} Hz for x=0.30, both below the Debye frequency. Moreover, these frequencies are close to the frequency of the Raman modes at ~80 cm^{-1} as shown in Fig. 2. In general, a dielectric relaxation below the optical phonon frequency range (ignoring piezoelectric resonances and domain wall motion) is a manifestation of some disorder in a dielectric material.[22] Although a process involving hopping of atoms is influenced by all phonons from the dispersion branch in the entire Brillouin zone, it is mostly affected by phonons of the lowest frequency phonon branches associated with O-A-O bending modes. Hence, the new low frequency Raman modes can be associated to a local change in polarisation due to defect-dipole reorientation.

An alternative explanation can be based on the mechanism proposed by Skanavi et al[23] for the relaxation observed in bismuth strontium titanate solutions. Basically, this model postulates that the distortions introduced by doping are sufficient to produce more than one off-center equilibrium position for the Ti^{4+} ion, and that the observed relaxation is associated with thermally activated motion between these equivalent minima. At this stage, the exact nature of the high temperature relaxation in BBTL ceramics is not fully understood and it will be subject of further investigations at our laboratory.

The results above show the dielectric behaviour of $Ba_{1-x}Bi_xTi_{1-x/3}Li_{x/3}O_3$ ($x \geq 0.20$) to be characterised by two large dielectric relaxations. To our knowledge, this is the first observation of double relaxor behaviour in a $BaTiO_3$-based solid solution.

Conclusions

Substitutional doping of $BaTiO_3$ with $Bi(Li_{1/3}Ti_{2/3})O_3$ according to the $Ba_{1-x}Bi_xTi_{1-x/3}Li_{x/3}O_3$ mechanism is accompanied by a change on the average crystal symmetry from tetragonal to cubic at $x > 0.10$. Nevertheless, changes to the local structure occur at even lower x contents as revealed by Raman spectroscopy analysis. Indeed, the presence of a lone-pair of electrons in Bi^{3+} affects the vibrations of the BO_3, whereas the presence of Li^{1+} in the B-site leads to a new high frequency phonon associated with the breathing of the oxygen octahedra. These changes to the vibrational properties are also accompanied by the emergence of a weak relaxor ferroelectric behaviour near room temperature and a secondary relaxor peak at higher temperatures. This latter phenomenon obeys the Arrhenius law and its activation energy of ~0.7 eV is consistent with either a defect-dipole reorientation or a Skanavi-type mechanism.

References

1 G Schileo, A Feteira, K Reichmann, M Li, and DC Sinclair, Journal of the European Ceramic Society **35** (9), 2479 (2015).

2 RE Cohen, Nature **358**, 136 (1992).

3 M Deluca, CA Vasilescu, AC Ianculescu, DC Berger, CE Ciomaga, LP Curecheriu, L Stoleriu, A Gajovic, L Mitoseriu, and C Galassi, Journal of the European Ceramic Society **32** (13), 3551 (2012).

4 A Feteira, DC Sinclair, IM Reaney, and MT Lanagan, Journal of the American Ceramic Society **88** (11), 3055 (2005).

5 H Ogihara, CA Randall, and S Trolier-McKinstry, Journal of the American Ceramic Society **92** (1), 110 (2009).

[6] T Strathdee, L Luisman, A Feteira, and K Reichmann, Journal of the American Ceramic Society **94** (8), 2292 (2011).
[7] L Luisman, A Feteira, and K Reichmann, Applied Physics Letters **99** (19) (2011).
[8] D Schuetz, M Deluca, W Krauss, A Feteira, T Jackson, and K Reichmann, Advanced Functional Materials **22** (11), 2285 (2012).
[9] K Datta, K Roleder, and PA Thomas, Journal of Applied Physics **106** (12), ARTN 123512 (2009).
[10] A Pinczuk, W Taylor, E Burstein, and I Lefkowitz, Solid State Communications **5** (5), 429 (1967).
[11] DY Lu, XY Sun, and M Toda, Journal of Physics and Chemistry of Solids **68** (4), 650 (2007).
[12] A Feteira, DC Sinclair, and J Kreisel, Journal of the American Ceramic Society **93** (12), 4174 (2010).
[13] A Feteira and DC Sinclair, Journal of Materials Chemistry **19** (3), 356 (2009).
[14] J Pokorny, UM Pasha, L Ben, OP Thakur, DC Sinclair, and IM Reaney, Journal of Applied Physics **109** (11), ARTN 123512 (2011).
[15] V Buscaglia, S Tripathi, V Petkov, M Dapiaggi, M Deluca, A Gajovic, and Y Ren, Journal of Physics-Condensed Matter **26** (6), ARTN 123512 (2014).
[16] M Deluca, G Picht, MJ Hoffmann, A Rechtenbach, J Topfer, FH Schader, and KG Webber, Journal of Applied Physics **117** (13), ARTN 134110 (2015).
[17] G Schileo, L Luisman, A Feteira, M Deluca, and K Reichmann, Journal of the European Ceramic Society **33** (8), 1457 (2013).
[18] WL Warren, K Vanheusden, D Dimos, GE Pike, and BA Tuttle, Journal of the American Ceramic Society **79** (2), 536 (1996).
[19] I Fujii, M Ugorek, YS Han, and S Trolier-McKinstry, Journal of the American Ceramic Society **93** (4), 1081 (2010).
[20] SH Cha and YH Han, Japanese Journal of Applied Physics Part 1-Regular Papers Brief Communications & Review Papers **45** (10A), 7797 (2006).
[21] O Bidault, P Goux, M Kchikeck, M Belkaomi, and M Maglione, Physical Review B **49** (12), 7868 (1994).
[22] S Kamba, V Porokhonskyy, A Pashkin, V Bovtun, J Petzelt, JC Nino, S Trolier-McKinstry, MT Lanagan, and CA Randall, Physical Review B **66** (5) (2002).
[23] GI Skanavi, IM Ksendzov, VA Trigubenko, and VG Prokhvatilov, JETP **6**, 250 (1958).

List of Figures

Figure 1. Room-temperature XRD data for $Ba_{1-x}Bi_xTi_{1-x/3}Li_{x/3}O_3$ ($0 \leq x \leq 0.30$) ceramics (increasing x from bottom to top).

Figure 2. Room-temperature Raman spectra for $Ba_{1-x}Bi_xTi_{1-x/3}Li_{x/3}O_3$ ($0 \leq x \leq 0.30$) ceramics (increasing x from bottom to top).

Figure 3. Temperature dependence of the (a) relative permittivity and (b) dielectric loss at 1 MHz for $Ba_{1-x}Bi_xTi_{1-x/3}Li_{x/3}O_3$ ($0 \leq x \leq 0.30$) ceramics.

Figure 4. Temperature dependence of the (a) relative permittivity and (b) dielectric loss for $Ba_{1-x}Bi_xTi_{1-x/3}Li_{x/3}O_3$ ceramics (x=0.20).

Figure 5. Temperature dependence of the (a) relative permittivity and (b) dielectric loss for $Ba_{1-x}Bi_xTi_{1-x/3}Li_{x/3}O_3$ ceramics (x=0.30).

Figure 6. Arrhenius representation of relaxation in $Ba_{1-x}Bi_xTi_{1-x/3}Li_{x/3}O_3$ ceramics (x=0.20 and 0.30).

List of Tables

Table I. Lattice parameters and unit cell volumes for $Ba_{1-x}Bi_xTi_{1-x/3}Li_{x/3}O_3$ ($0 \leq x \leq 0.30$) ceramics.

Table I

Composition, x	a (Å)	b (Å)	c/a	Volume (Å^3)
0	3.9903(6)	4.0314(9)	1.0103	64.189(15)
0.05	3.9930(8)	4.0349(9)	1.0105	64.301(16)
0.10	3.9984(5)	4.0370(7)	1.0097	64.541(12)
0.20	4.0075(4)			64.363(12)
0.30	4.0081(6)			64.388(16)

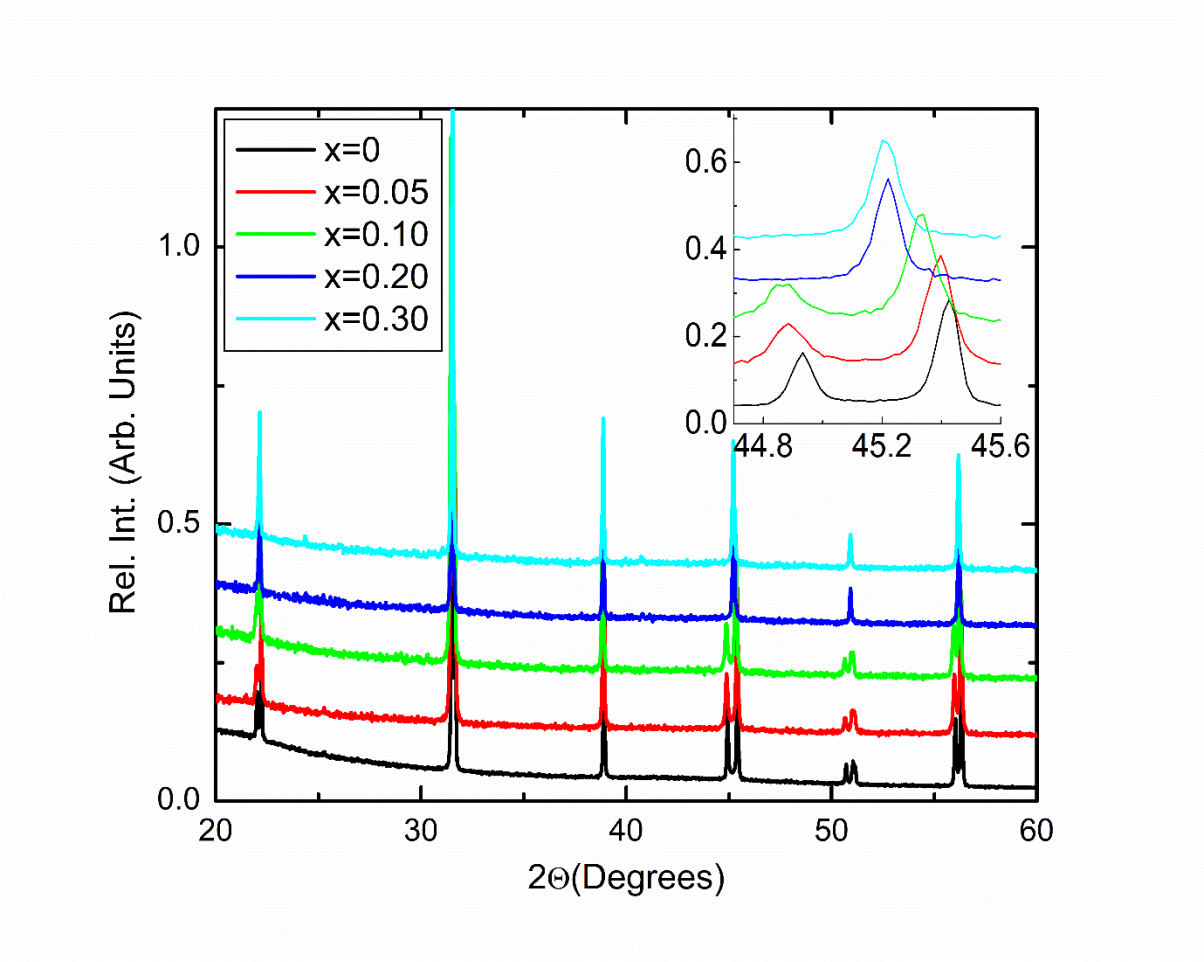

Fig. 1

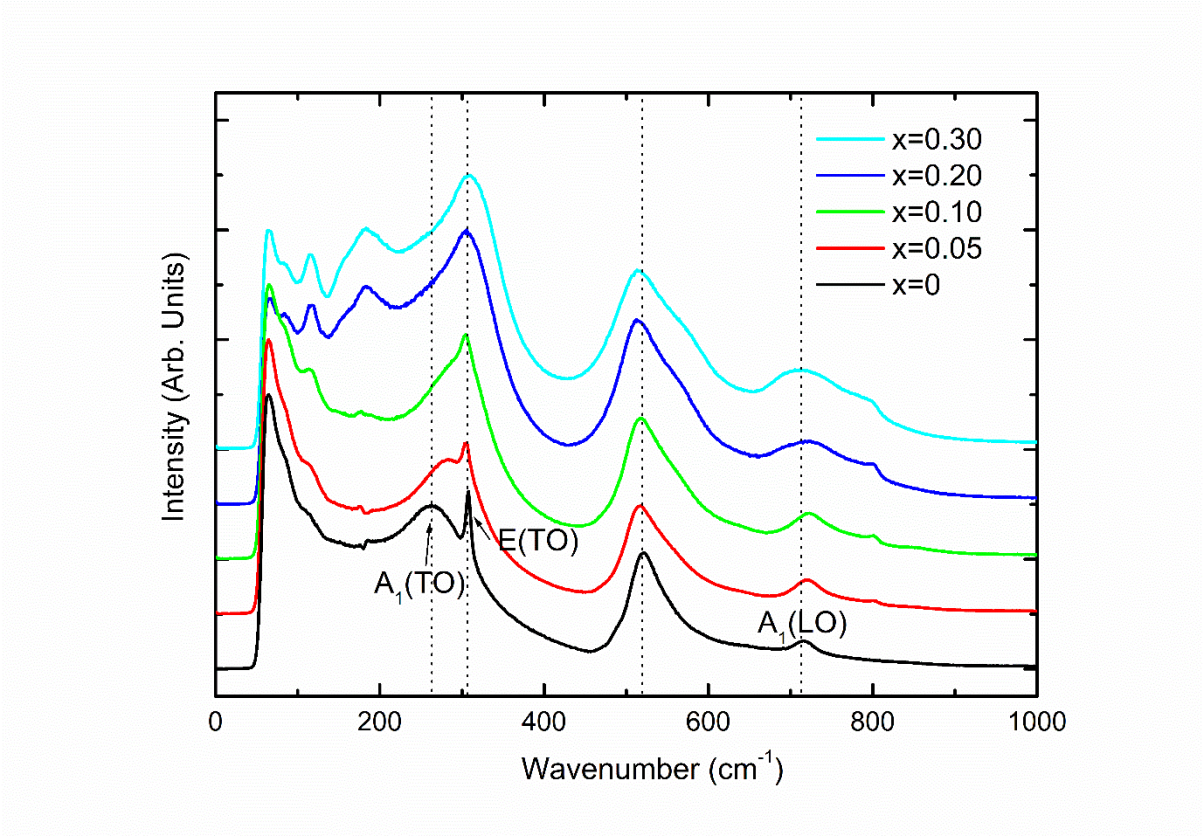
x=0.30
x=0.20
x=0.10
x=0.05
x=0
Intensity (Arb. Units)
A1(TO)
E(TO)
A1(LO)
0
200
400
600
800
1000
Wavenumber (cm-1)

Fig. 2

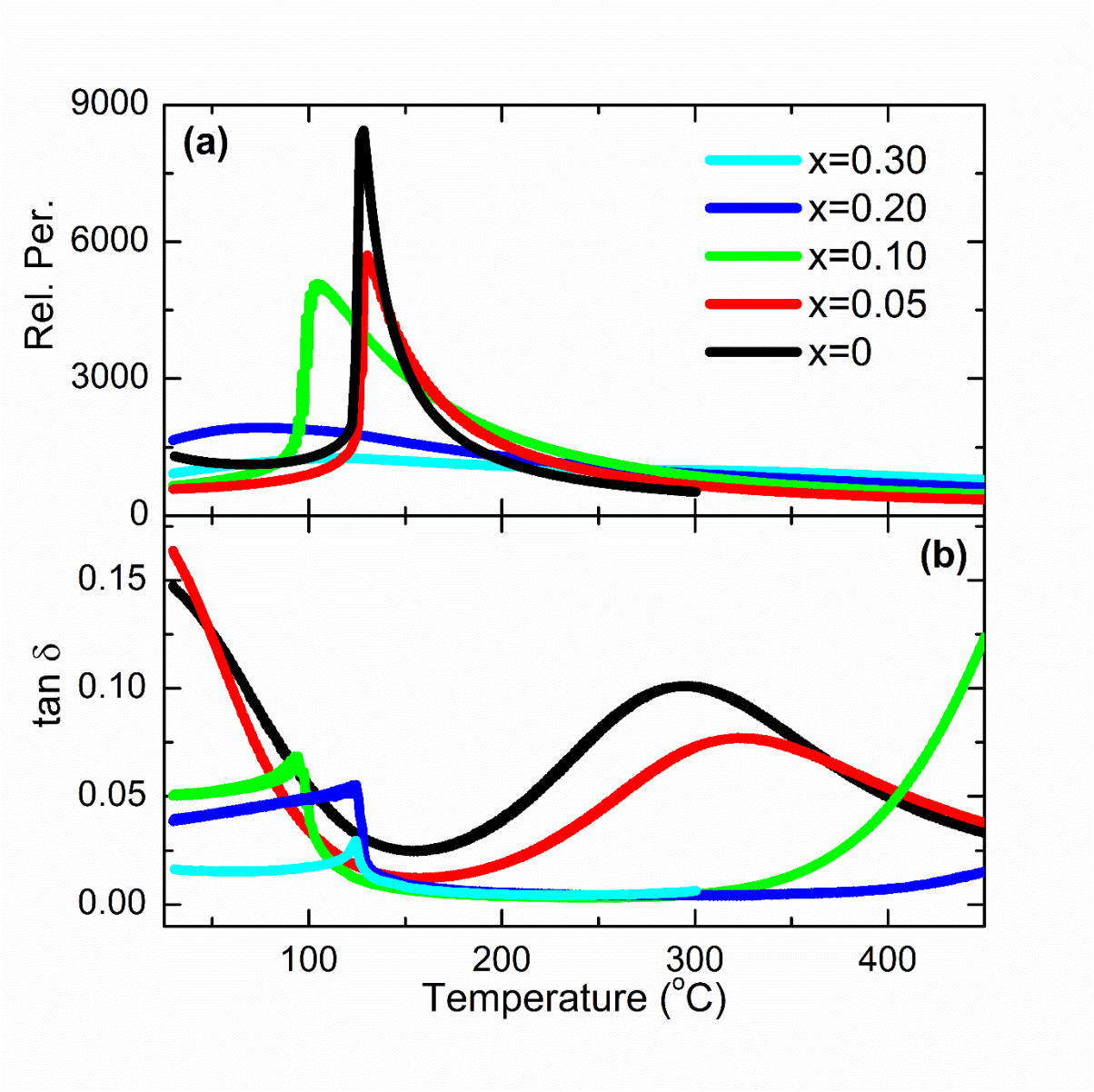
(a)
(b)
Rel. Per.
tan δ
Temperature (°C)
x=0.30
x=0.20
x=0.10
x=0.05
x=0
9000
6000
3000
0
0.15
0.10
0.05
0.00
100
200
300
400

Fig. 3

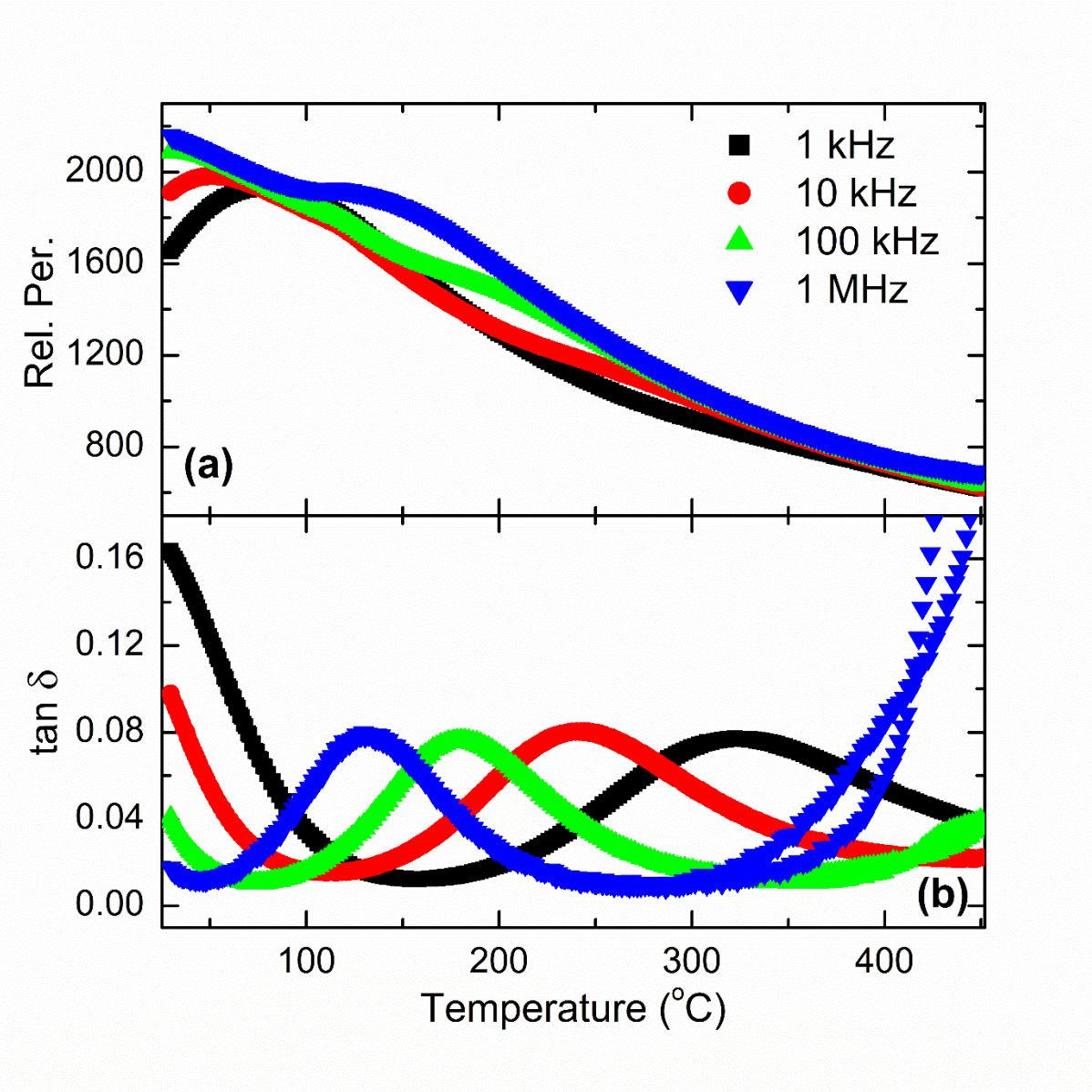
1 kHz
10 kHz
100 kHz
1 MHz
Rel. Per.
2000
1600
1200
800
(a)
tan δ
0.16
0.12
0.08
0.04
0.00
(b)
100
200
300
400
Temperature (°C)

Fig. 4

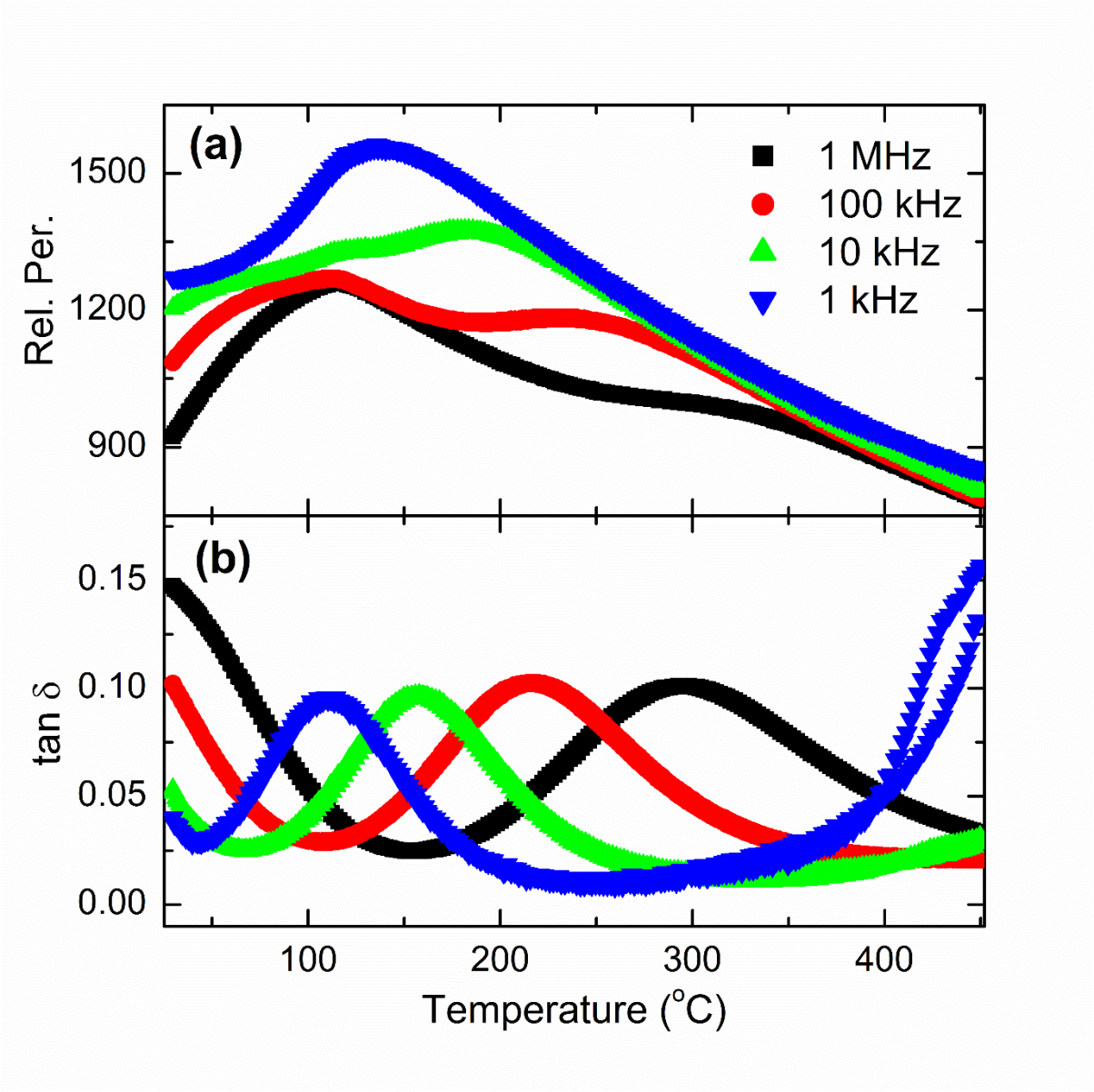
(a)
1 MHz
100 kHz
10 kHz
1 kHz
Rel. Per.
1500
1200
900
(b)
tan δ
0.15
0.10
0.05
0.00
100
200
300
400
Temperature (°C)

Fig. 5

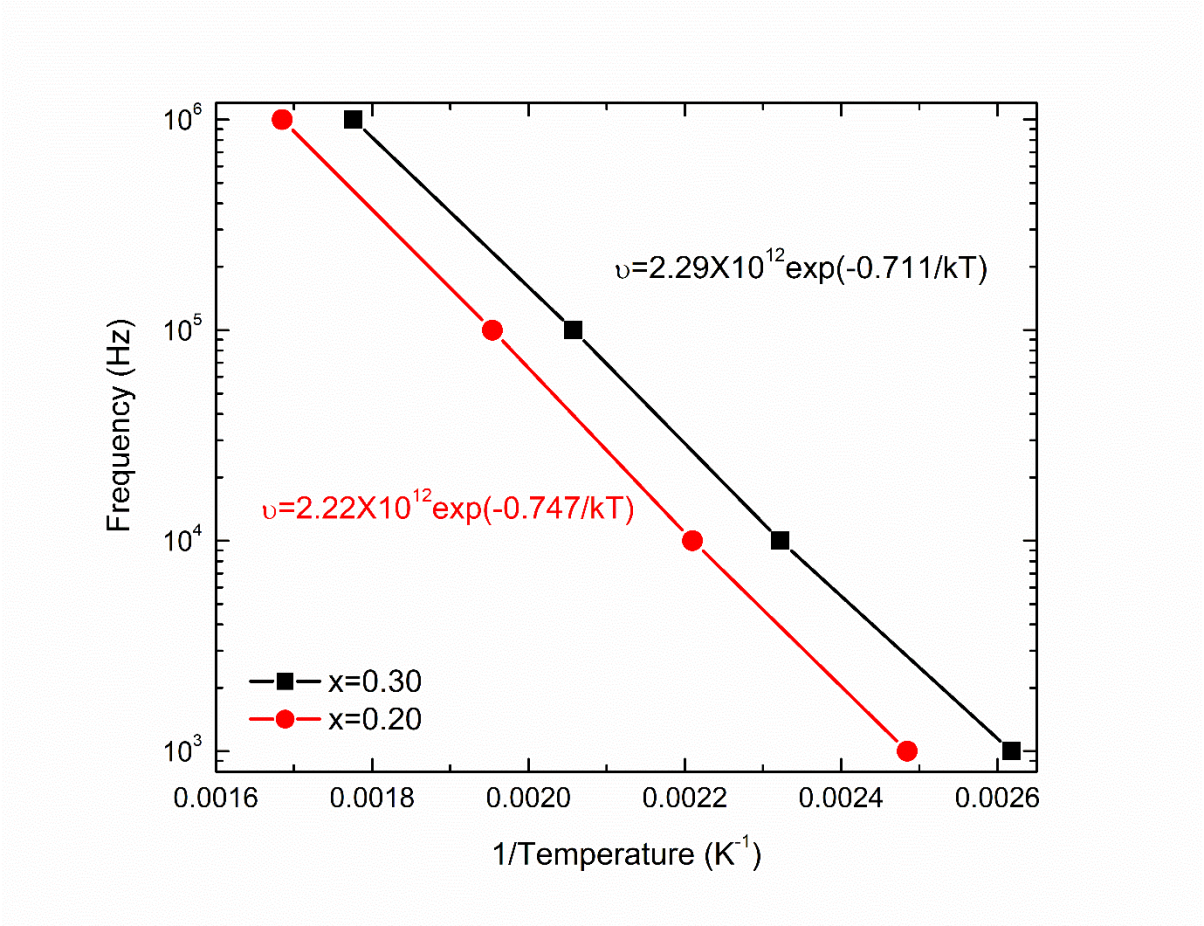
Frequency (Hz)
10^6
10^5
10^4
10^3
υ=2.29X10^12exp(-0.711/kT)
υ=2.22X10^12exp(-0.747/kT)
x=0.30
x=0.20
0.0016
0.0018
0.0020
0.0022
0.0024
0.0026
1/Temperature (K^-1)

Fig .6